Hindawi
Journal of Nanomaterials
Volume 2022, Article ID 8800117, 18 pages
https://doi.org/10.1155/2022/8800117

Research Article

Thiourea-Mediated Reduced Graphene Oxide Nanosheets, Their Cytotoxic Impacts on Human Prostate Cancer Cells, and Their Antibacterial Effects against *E. coli* Mastitis

Babu Vimalanathan,[1] Judith Vijaya J,[2] Stephen Selvamani P,[2] Manivannan,[3] Savarimuthu Ignacimuthu,[4] Magesh Daniel,[5] Mohamed Bououdina,[6] and Jayavel Ramasamy[1]

[1]*Crystal Growth Centre, Anna University, Chennai, 600 025 Tamil Nadu, India*
[2]*Catalysis and Nanomaterials Research Laboratory, Department of Chemistry, Loyola College, Chennai 600 034, India*
[3]*Department of Physics, National Institute of Technology, Tiruchirappalli, 620015 Tamil Nadu, India*
[4]*Xavier Research Foundation, St. Xavier's College, Palayamkottai, 627002 Tamil Nadu, India*
[5]*Department of Zoology, Loyola College, Chennai, 600 034 Tamil Nadu, India*
[6]*Department of Mathematics and Science, Faculty of Humanities and Sciences, Prince Sultan University, Riyadh, Saudi Arabia*

Correspondence should be addressed to Judith Vijaya J; jjvijaya78@gmail.com and Jayavel Ramasamy; rjvelsms@gmail.com

Received 7 June 2022; Revised 16 August 2022; Accepted 25 August 2022; Published 20 September 2022

Academic Editor: Dong Kee Yi

This study was aimed at determining the cytotoxic efficacy of graphene oxide (GO) and thiourea-reduced oxide (T-rGO) nanosheets against human prostate cancer cells and their antibacterial activity against *E. coli* mastitis. X-ray diffraction, Raman spectroscopy, Fourier transformed infrared spectroscopy, and scanning electron microscopy were used to study the physicochemical properties of the fabricated GO and T-rGO. The cytotoxicity of GO and T-rGO in human prostate cancer cells was examined using cell survival test, DNA laddering, and cell cycle analysis. The antibacterial effectiveness of GO and T-rGO was tested using *E. coli* mastitis. The study revealed that cell viability was lowered by GO and T-rGO in a concentration-dependent trend. The production of reactive oxygen species and hydroxyl radicals was found to increase following the treatment. DNA was harmed because of oxidative stress, causing laddering. Both GO and T-rGO demonstrated good antibacterial activity against *E. coli* mastitis. The findings of this research work provide insightful information about functional graphene derivatives for potential biomedical applications, primarily cancer treatment.

1. Introduction

Nanotechnology is now the most prospective sector for developing novel biotechnological and nanomedical applications [1]. Graphene is a carbon atom monolayer [2, 3] that is single and closely packed. Even though graphene-like structures had been researched since the mid-twentieth century [4–6] and free-standing ultrathin graphene sheets were photographed in 1962 by Boehm et al. [3], massive single-layered graphene sheets were not successfully isolated until 2004 [7, 8]. Since its discovery in 2004 [7] by K.S. Novoselov and A.K. Geim, graphene has attracted great interest, thanks to its intriguing and fascinating physiochemical properties such as fracture strength [9], high surface area [10, 11], mobility of charge carriers [12], outstanding electrical conductivity [13], resilient mechanical strength [14], exceptional thermal conductivity [15], and facile functionalization [16, 17]. As components in devices, graphene and chemically modified graphene are potentially utilized in diverse applications in energy-storage [18] foam [19], paper-like substances

[20, 21], polymer composites [22, 23], liquid crystal device [24], and mechanical resonators [25].

Graphene oxide (GO) and reduced graphene oxide (rGO) have shown interesting antibacterial activity [26]. Membrane stress is caused by the sharp edges of graphene nanosheets and consequently induces physical damage to cell membranes, jeopardizing bacterial membrane integrity and permitting RNA leakage [27].

Drug/gene delivery, cancer therapy, biosensing, bioimaging, scaffold for cell culture [28], stem cell biology [29], antiviral [30], and tissue engineering [31–33] are just a few of the medical and biological applications for graphene and its derivatives. Besides these, few studies investigated their biomedical applications such as medication loading and delivery [34, 35].

Sun et al. and Liu et al. investigated PEGylated nanoscale graphene oxide as a nanocarrier to load anticancer drugs into cells via noncovalent physisorption [34, 35]. Further, graphene-based materials demonstrated exceptional electrochemical and optical properties, as well as the ability to adsorb a wide range of aromatic biomolecules through either stacking or electrostatic contact. This makes them suitable materials for attaching functional groups consisting of oxygen to their honeycomb, such as six-atom carbon rings. To help targeted imaging and medicine delivery, graphene oxide can be easily changed with a targeting ligand [36].

According to Lulu et al. [37], GO-PLL-SDGR-functionalized graphene oxide was examined as a nonviral tumor targeting carrier in si-RNA delivery systems to actively target tumors. Ting et al. [38] reported that chitosan- (CS-) functionalized GO (GO-CS) strongly activated RAW 264.7 cells and triggered more cytokines, thereby facilitating cellular immune response. This was attributed to the synergistic immune stimulatory impact of GO and CS. The as-fabricated GO-CS proved to be a promising nanoadjuvant for vaccinations and immunotherapy.

According to the World Health Organization (WHO), prostate cancer is the world's fifth most prevalent cancer, the second most common malignancy in men, and the second leading cause of cancer death [39–41]. On the other hand, mastitis is the most costly and economically destructive disease in the dairy business. Physical, chemical, and generally bacteriological alterations in milk, as well as pathological abnormalities in glandular tissues and leukocytes, characterize this inflammation of the mammary glands [42, 43]. Bovine mastitis is the most frequent infectious disease that affects dairy cows, and it limits the production of various dairy products [44]. Treatment costs, milk disposal due to high bacterial load, milk production reduction, culling of high-producing affected animals, and additional labor costs while handling affected animals are all elements that contribute to the high-cost involvement [45].

In this regard, the development of new medicines for prostate cancer and mastitis is critical. Future research on new anticancer drugs could benefit greatly from the use of grapheme nanosheets. Thiourea's chemical structure makes it an excellent reducing and effective capping agent simultaneously.

The first objective of this study consists of using thiourea to synthesize and characterize graphene derivatives, namely, graphene oxide (GO) and reduced graphene oxide (rGO). The second objective is to determine if GO and rGO may be cytotoxic to human prostate cancer cells and the E. coli mastitis bacterium, which is frequently utilized in research on cytotoxicity, oxidative stress, cancer, and bacterial infections. Furthermore, determining the cytotoxicity/toxicity of reduced graphene oxide and GO on human prostate cancer cells and the E. coli mastitis bacteria is the study's primary aim. The new aspect of this work is the modified Hummers method adopted to manufacture GO from raw graphite powder and oxidants like $KMnO_4$, $NaNO_3$, and 98 percent H_2SO_4. This paper presents a straightforward and cost-effective method for producing water-soluble rGO from thiourea, which has a wide range of medicinal uses. Besides, the drawbacks of traditional chemotherapy treatments for cancer are the lack of selectivity, systemic toxicity, and chemoresistance. More precise and targeted cancer treatment using nanomaterials like graphene derivatives could successfully reduce negative side effects while providing accurate diagnosis and efficient therapy.

2. Materials and Methods

The graphite powder was purchased from Sigma-Aldrich. Analytical grade NaOH, thiourea, $KMnO_4$, anhydrous ethanol, H_2SO_4 98%, HCl 36%, and hydrogen peroxide (H_2O_2) 30% were also obtained from Sigma-Aldrich. All reagents were used without further purification. Deionized water (DW) was used to prepare all aqueous solutions. The remaining chemicals were also purchased from Sigma-Aldrich unless otherwise specified.

2.1. Synthesis of GO. Graphite oxide was produced by the modified Hummers' method [46] using graphite as raw material with $KMnO_4$, $NaNO_3$, and 98% H_2SO_4 as oxidants.

2.2. Synthesis of T-rGO. 500 mg of GO was dispersed in 250 mL water using ultrasonication for 1 h and 30 min to generate GO dispersion. After that, 500 mg of thiourea was added to the dispersion under stirring and refluxed at 94°C for 24 h in a typical reduction experiment. The brown color of the GO dispersion changed to black after the reduction process.

2.3. Characterization. As previously described [47–49], the crystalline structure of GO and T-rGO was checked by powder X-ray diffraction using Rigaku Miniflex II-C equipped with Cu-Kα radiation ($\lambda = 0.15406$ nm). Raman spectra were recorded at room temperature with an excitation wavelength of 532 nm using Agiltron Peak Peaker Pro 532. Morphological observations were carried out by scanning electron microscopy using Tescan Vega 3, Czech Republic nation. Prior to imaging, GO and T-rGO powders were fixed onto an Al sample holder and then coated with gold. The nature of bonds and functional groups were determined by Jasco FTIR 6600FT-IR spectrometer, using KBr pellets. The sample's thermal stability was investigated using an EXSTAR SII TG/DTA 6300 and thermogravimetric analysis

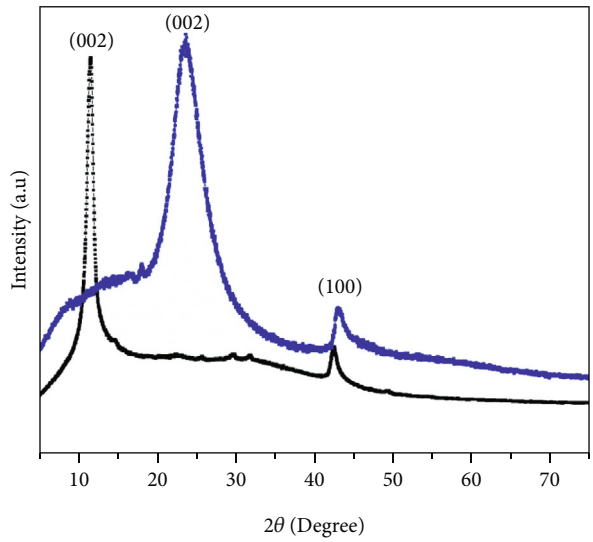

Figure 1: XRD patterns of GO and T-rGO.

(TGA) under nitrogen environment, up to1000°C at a heating rate of 10°C/min.

2.4. Cell Line and Culture. The NCCS in Pune, India, provided the human prostate cancer cell line PC3. When the cells reached 80 percent confluence, they were passaged every three to five days with 0.25% trypsin and 0.05% ethylene diamine tetra acetic acid (EDTA) solution. The cultivation of the cells was carried out in F-12 K medium, and the incubation was performed under 5% CO_2 atmosphere at 37°C using a ThermoFisher Scientific (India) incubator. In Kaighn's modified Ham's F-12 medium, 2 mM of L-glutamine, 10% fetal bovine serum, 1500 mg/L sodium bicarbonate, and 1% penicillin-streptomycin (100 U/mL streptomycin and 100 U/mL penicillin) were used [50, 51].

2.5. Reagents. HiMedia Laboratories provided Kaighn with its modified Ham's F-12 medium. Cistron Laboratories provided the fetal bovine serum (FBS). Trypsin water-soluble tetrazolium salt (WST-8) and dimethyl sulfoxide were provided by Sisco Research Laboratory Chemicals, Mumbai (DMSO). Sigma-Aldrich, Mumbai, provided the additional reagents and chemicals.

2.6. Cell Culture and Exposure to GO and T-rGO. The cell culture was performed as described in the literature [50, 51]. Human prostate cancer cells (PC-3) were cultured in Kaighn's modified Ham's F-12 medium with 10% FBS, 2 mM glutamine, and 100 U/mL penicillin-streptomycin in a humidified 5% CO_2 incubated at 37°C. The medium was supplied three times a week, and the cells were passaged at subconfluence. The cells were harvested at roughly 75% confluence using 0.25 percent trypsin-EDTA and seeded in 75 cm^2 flasks, 96-well plates, or 6-well plates, depending on the study. The medium was replenished after 24 h with fresh medium and varied concentrations of GO and T-rGO (1000-7.8 μg/mL); the cells without GO and T-rGO were used as control. The vitality of the treated cells, DNA fragmentation, cell cycle pattern, and cell morphology were tested after 24 h incubation period.

2.7. WST-8 Cell Viability Assay. The WST-8 assay was used to determine cell viability, as previously described [52, 53]. In a 96-well plate, 1×10^4 cells (human prostate cancer PC-3 tumor) were planted in 100 μL Ham's F-12 medium containing 10% FBS. The cells were then washed twice with 100 μL serum-free Ham's F-12 medium and incubated in 100 μL serum-free Ham's F-12 medium containing varying concentrations of GO or T-rGO suspensions. After 24 h of exposure, the cells were washed twice with serum-free Ham's F-12 medium. The WST-8 solution was then applied to each well containing 100 μL serum-free Ham's F-12 medium. After 1 h of incubation, 80 μL of the mixture solution was transferred to another 96-well plates to avoid residual GO or T-rGO affecting the absorbance at 450 nm using a microplate reader. To determine if GO and T-rGO reacted directly with the WST-8 reagent, cell-free control tests were carried out. Typically, 100 μL of GO or T-rGO suspensions with varying concentrations were placed into 96-well plate, with 10 μL WST-8 reagent solution added to each well; this mixed solution was incubated at 37°C for 1 h under 5% CO_2. Then, they were centrifuged after incubation, and 50 μL of each supernatant was transferred to a new 96-well plate. At 450 nm, the optical density was observed.

2.8. Cell Cycle Analysis. In 6-well plates, 2×10^5 human prostate cancer cells were platted and cultured for 24 h. After having been treated with IC_{50} doses of GO (125 μg/mL) and T-rGO (62.5 μg/mL), the monolayer of cells was grown for 24 h. The treated cells were centrifuged after being washed with sterile PBS. The cells were then given 0.2 mL of propidium iodide (10 μg/mL) and incubated for 30 min. Flow cytometry was used to observe at 488 nm [54].

2.9. DNA Fragmentation. The platting of 2.0×10^5 human prostate cancer cells was carried out in 6-well plates and cultured in a CO_2 incubator to achieve convergence. The cells were treated with different quantities of GO (IC_{50} concentration of 125 μg/mL) and T-rGO (IC_{50} concentration of 62.5 μg/mL) after they reached confluence. After collecting the cells with TPVG, the cell suspension of 1.5 mL was put into an Eppendorf tube. After that, centrifugation of the cells was carried out for 10 min at 200 × g and 4°C. Then, the pellet was vortexed vigorously with 0.5 mL TTE solution. This technique facilitated the release of fragmented chromatin from nuclei as well as the breakdown of nuclear structure (due to Mg^{++} chelation by EDTA in the TTE solution) post cell lyses (because of the existence of Triton X-100 in the TTE solution). The centrifugation of solution was performed at 20,000 g for 10 min at 4°C in order to isolate split DNA from undamaged chromatin. The supernatant was then discarded with care, and TTE solution of 500 μL was supplemented to the particle. After that, 500 μL of ice-cold NaCl was supplied and vigorously refluxed. After the salt was introduced, histones were stripped from DNA. After that, ice-cold isopropanol of 700 μL was supplied and violently refluxed; this was then let to precipitate overnight at -20°C.

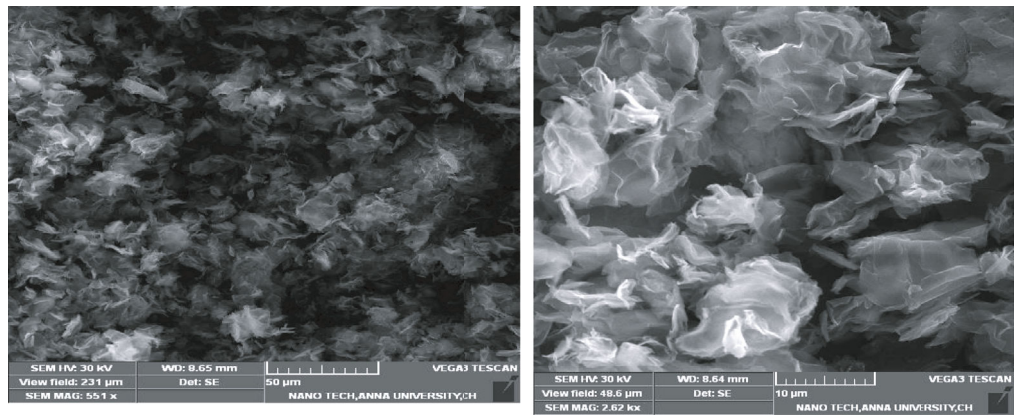

Figure 2: SEM images of GO and T-rGO.

The DNA pellet was recovered by centrifuging at 20,000 *g* for 10 min at 4°C and rinsing with 500–700 μL of ice-cold 70% ethanol. This was centrifuged for 10 min at 20,000 *g* at 4°C. The DNA pellet was dissolved in 20–50 μL of TE buffer and kept at 4°C. Electrophoresis of this DNA was performed in normal TE buffer. To achieve a final concentration of 1×, the DNA was combined with loading buffer (10×) and bromophenol blue dye. This made loading samples into the wells and monitoring their mobility over the gel easier. The electrophoresis was terminated after the dye reached about 3 cm from the end of the gel. To visualize the gel, a UV transilluminator was employed [55, 56].

2.10. Cell Morphology. Human prostate cancer cells (1×10^5 cells per well) were planted in 6-well plates and kept for 24 h. The cells were cultivated in GO (IC_{50} concentration) concentrations of 1000, 125, and 7.8 μg/mL and then in T-rGO concentrations of 1000, 62.5, and 7.8 μg/mL (IC_{50} concentration). As control, the cells cultivated without GO and T-rGO were employed. After 24 h of exposure, the morphology of the cells was evaluated under an optical microscope [57].

2.11. Isolation of the Bacterium. Milk samples were collected from a dairy cow with clinical mastitis (veterinary diagnosis done at Department of Clinical Microbiology, Madras Veterinary College, and Chennai, India). The samples were analyzed for the presence of *Escherichia coli* (*E. coli*). A mix of cultural, morphological, and biochemical methods was used to localize the bacteria. Microscopic examination was performed after 24 h on blood agar plates. Oxidase, catalase, and indole tests were carried out.

2.12. Characterization of the Isolate. The pathogen *E. coli* was used in this study, which was isolated from a clinical instance of cow mastitis. Cultural and biochemical features verified the strain; it was kept in slants till further usage [58].

2.13. Media Preparation and Bacterial Growth Analysis. The method of Gurunathan et al. [59] was used for media preparation and bacterial growth analysis. In a nutshell, *E. coli* was grown under aerobic conditions at 37°C in Luria-Bertani (LB) broth comprising of 20 g of tryptone, 15 g of extract of yeast, and 10 g of sodium chloride per L of mastitis-affected cow milk. To attain the required initial optical density, the cells were collected by centrifugation, rinsed thoroughly with phosphate-buffered saline (PBS; pH 7.3), and reconstituted in suitable fresh medium such as LB or saline. The introduced cultures were cultured in 50 mL tubes in a shaker (120 rpm) at 37°C till they reached a stationary phase (tube volume/medium volume -1/10). By measuring the absorbance at 600 nm on a regular basis, the growth was measured. The cultivation of bacteria was carried out on LB agar slants and kept in a glycerol stock solution at -70°C. Complete experiments were carried out three times independently, unless specified otherwise.

2.14. Turbidity Assay. By means of a UV spectrophotometer, bacterial culture was assessed based on its turbidity at OD600. In LB medium, *E. coli* was treated with GO and T-rGO. As a control, *E. coli* that had not been treated was employed. *E. coli* cells were spun down at 5000 rpm for 10 min and the supernatant was removed. The pellet (bacterial cells) was redissolved in PBS after the supernatant (soluble graphene components) was discarded. At 3 h intervals, the treated and untreated samples were monitored at 600 nm. For each experiment, three separate runs were carried out.

2.15. Cell Preparation. E. coli was isolated from mastitis-affected cow milk and cultured in LB medium at 37°C. During the midexponential growth phase, the cells were extracted. For 10 min, the cells were centrifuged at 6000 rpm. To eliminate leftover macromolecules and other growth medium elements, isotonic saline solution was used to wash the cells three times. The pelleted cells were then resuspended in an isotonic saline solution. Cell samples containing 10^6 to 10^7 CFU/mL were obtained by diluting bacterial cell suspensions.

2.16. Cell Viability. After treating the bacteria with GO and T-rGO, the vitality of the cells was evaluated. *E. coli* cells isolated from mastitis-affected cow milk were treated with GO and T-rGO at varied doses (0, 25, 50, 75, 100, 125, and 150 μg/mL) in isotonic saline solutions for 2 h at 37°C and

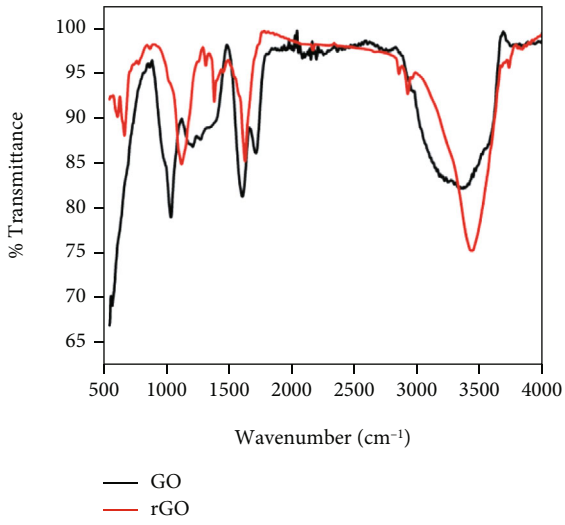

Figure 3: FTIR spectra of GO and T-rGO.

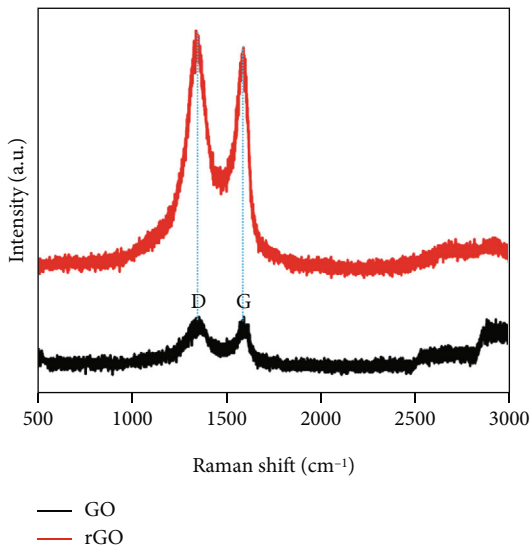

Figure 4: Raman spectroscopy analysis of GO and T-rGO.

200 rpm. Isotonic saline solution without GO and T-rGO was used as control. Following the treatment, the reaction mixture of 100 μL was made up to 1 mL, from which 50 μL was used for plating. The method of colony counting was used to assess the vitality of *E. coli* cells. 100 μL each of tenfold dilutions was cultured overnight at 37°C on LB plates. The colonies on the test plates were quantified and contrasted with those on the control plates. All the treatments were carried out in duplicate three times.

2.17. Observation of Cell Morphology. Cell suspensions of *E. coli* were subjected to silicon wafers and exposed to 1% osmium tetroxide and 2% glutaraldehyde. After that, dehydration of the cells was carried out in ethanol concentrations ranging from 30, 50, 70, 80, 90, and 100% for 15 min. The sputter-coating of dried cells with gold was performed for SEM imaging using JEOL field emission SEM (JSM-6700F).

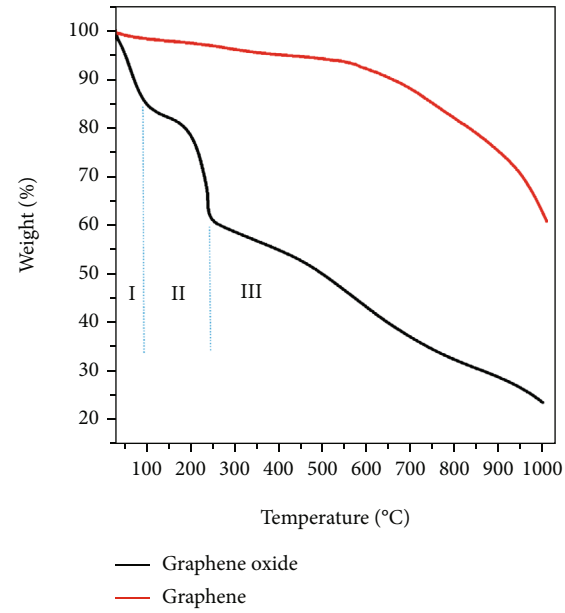

Figure 5: Thermogravimetric analysis of GO and T-rGO.

2.18. Measurement of ROS Generation. The quantitative analysis of superoxide anions was conducted according to the assembly specifications. Sigma-Aldrich (catalogue number TOX2) provided the *in vitro* toxicology assay kit (based on sodium 2,3,bis(2-methoxy-4-nitro-5-sulfophenyl)-5-(phenylamino)-carbonyl-2H-tetrazolium inner salt (XTT). The culturing of *E. coli* cells was carried out in LB medium, rinsed in PBS, and resuspended at a density of 2×10^8 potential cells/1 mL in PBS. From a stock solution, XTT was mixed with the cell lysate at a dosage of 125 M (7.5 mM made in PBS). The culturing of cell suspensions was performed on a rotating shaker at 30°C for the durations specified (2 and 4 h). The supernatants were utilized to measure the absorbance at 450 nm after the serial dilutions were whirled in a microfuge. Reducing XTT was the control used in the deficiency of cells.

2.19. DNA Laddering. The *E. coli* cells had been grown in LB medium, rinsed with PBS buffer, and then reconstituted in PBS at a dose of 2×10^8 inoculums. After being treated for 24 h with 100 μg/mL GO and T-rGO, the pellet was resuspended in 250 μL cell extraction buffer comprising 50 mM Tris–HCl, pH 8.0, 10 mM EDTA, 0.1 M NaCl, and 0.5% SDS. The homogenate was processed for 1 h at 37°C with 0.5 mg/mL RNase A and then overnight at 50°C with 0.2 mg/mL proteinase K.

Following phenol extraction, 25 mL (1/10 vol) of 7.5 M ammonium acetate and 250 mL (1/10 vol) of isopropanol were used to isolate DNA in the aqueous layer. Electrophoresis was carried out at 70 V in a 1% agarose gel comprising 1 mg/mL ethidium bromide, and DNA fragments were visible by presenting the gel to UV light. The photographs of the same were taken.

2.20. Physicochemical Properties

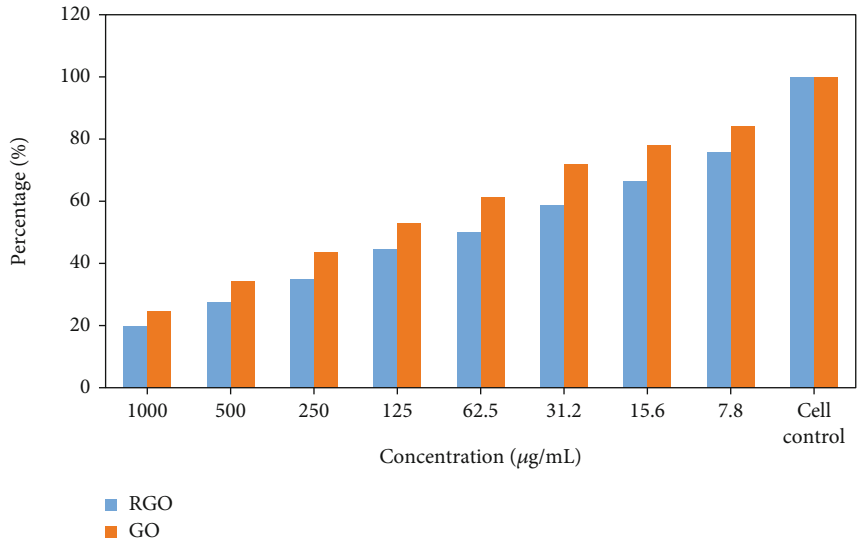

Figure 6: Effects of GO and T-rGO on cell viability of PC-3 human prostate cancer cells. The viability of PC-3 human prostate cancer cells was determined after 24 h exposure to different concentrations of GO and T-rGO using the WST-8 assay.

Table 1: Anticancer effect of GO on PC3 cell line.

Sample	Concentration (μg/mL)	Dilutions	Absorbance (O.D)	Cell viability (%)
1	1000	Neat	0.158	24.61
2	500	1 : 1	0.220	34.26
3	250	1 : 2	0.279	43.45
4	125	1 : 4	0.339	52.80
5	62.5	1 : 8	0.393	61.21
6	31.2	1 : 16	0.462	71.96
7	15.6	1 : 32	0.501	78.03
8	7.8	1 : 64	0.541	84.26
9	Cell control	—	0.642	100

Table 2: Anticancer effect of T-rGO on PC3 cell line.

Sample	Concentration (μg/mL)	Dilutions	Absorbance (O.D)	Cell viability (%)
1	1000	Neat	0.128	19.93
2	500	1 : 1	0.176	27.41
3	250	1 : 2	0.225	35.04
4	125	1 : 4	0.287	44.70
5	62.5	1 : 8	0.322	50.15
6	31.2	1 : 16	0.377	58.72
7	15.6	1 : 32	0.426	66.35
8	7.8	1 : 64	0.487	75.85
9	Cell control	—	0.642	100

2.20.1. X-Ray Diffraction Analysis. X-ray diffraction pattern (Figure 1) displays typical characteristic peaks of GO, i.e., (002) and (100) reflections located at 10.12° and 42.68°, respectively, in agreement with JCPDS card no. 75-2078 [60]. After thiourea reduction of graphene oxide (T-rGO), the main reflection (002) is shifted significantly to 25.18°, whereas (100) remain unchanged, in agreement with JCPDS card no. 03-0401 [61]. Furthermore, after reduction, the broadening of peaks becomes more important. The shift in position and broadening of the peaks may be associated with the reduction of graphene oxide to rGO using thiourea, and the above results corroborate well with the literature [62, 63].

2.20.2. SEM Observations. SEM images of GO and T-rGO are shown in Figure 2. On the surface of GO, a few layers of clustered, square molded, and folded sheets are seen securely connected with one another to form a regular loading network. The exterior layer of GO sheets has a thin floor cover in wavy shapes, perhaps because of the leftover water atoms present and hydroxyl or carboxyl collecting, revealing flimsy layers of nanosheets. The GO paper-like layers are stacked one on top of the other. SEM image of T-rGO's reveals simple and undulated silk wave morphology. The observed morphologies corroborate with the literature [64, 65].

2.20.3. FTIR Analysis. The FTIR spectra of GO and T-rGO are shown in Figure 3. The bands located at 3365, 1729, 1230 cm^{-1}, and 1035 cm^{-1} are assigned to the vibration and deformation of O-H groups, C=O stretching vibration, C-O (epoxy) stretching vibration, and C–O–C stretching, respectively. The above observed bands confirm the presence of several types of oxygen-containing species in GO. The FTIR spectroscopy of graphene is very different from that of GO. The FTIR spectrum of T-rGO's reveals primarily the presence of OH stretching band at 3424 cm^{-1}, signifying that GO has been significantly reduced throughout the deoxygenating process. The forces of assimilation tops comparing to oxygen practical gathering nearly disappeared. Overall, FTIR analysis demonstrates that during the reduction phase of GO, the oxygen-containing species have been totally removed [66, 67].

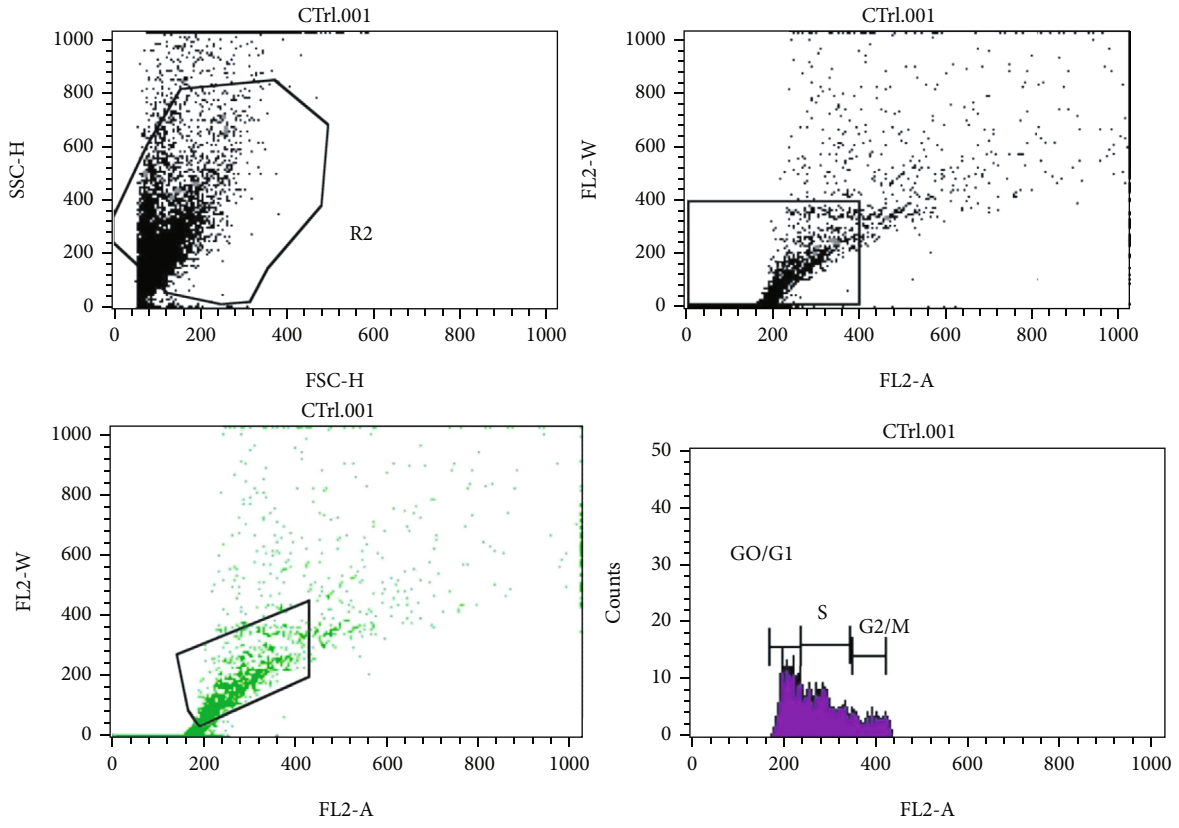

Histogram statistics

File: CTrl.001
Log data units: Linear values
Sample ID:
Patient ID:
Tube: Unititled
Panel: Untitled acquisition tube list
Acquisition Date: 21-Jun-18
Gate: G1
Gated events: 969
Total events: 10000
X Parameter: FL2-A (Linear)

Marker	Left, Right	Events	% Gated	% Total	Mean	Geo Mean	CV	Meadian	Peak Ch
All	0, 1023	969	100.00	9.69	266.35	259.67	23.28	252.00	192
GO/G1	168, 234	388	40.04	3.88	209.69	209.19	6.85	209.00	192
S	236, 342	436	44.99	4.36	281.26	279.73	10.52	278.50	253
G2/M	347, 418	118	12.18	1.18	381.46	380.86	5.63	381.00	386

(a) Control

Figure 7: Continued.

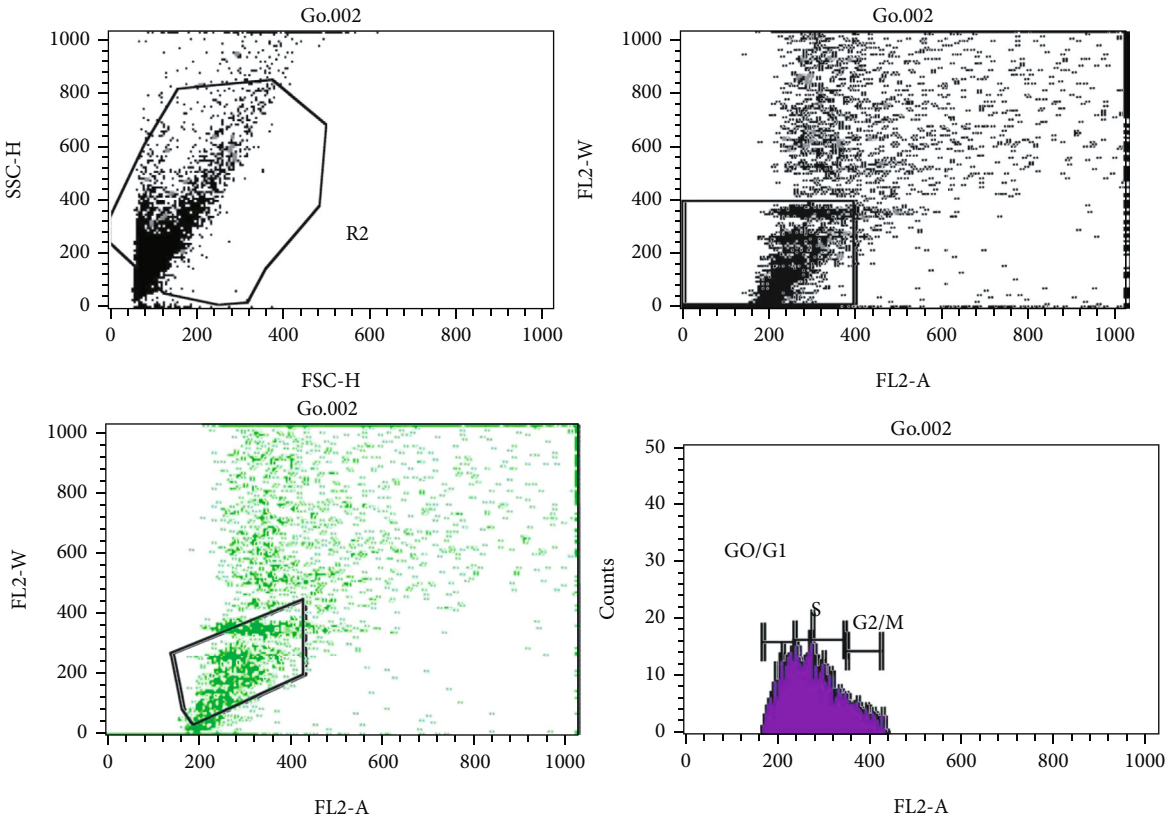

Histogram statistics

File: Go.002	Log data units: Linear values
Sample ID:	Patient ID:
Tube: Untitled	Panel: Untitled acquisition tube list
Acquisition date: 21-Jun-18	Gate: G1
Gated events: 1545	Total events: 10000
X Parameter: FL2-A (Linear)	

Martker	Left,	Right	Events	% Gated	% Total	Mean	Geo Mean	CV	Median	Peak Ch
All	0,	1023	1545	100.00	15.45	270.80	265.35	20.53	263.00	272
GO/G1	168,	234	462	29.77	4.60	211.12	210.54	7.32	213.00	231
S	236,	342	881	57.02	8.81	280.20	278.71	10.43	276.00	272
G2/M	347,	418	162	10.49	1.62	375.15	374.66	5.19	370.50	350

(b) GO-treated cells

Figure 7: Continued.

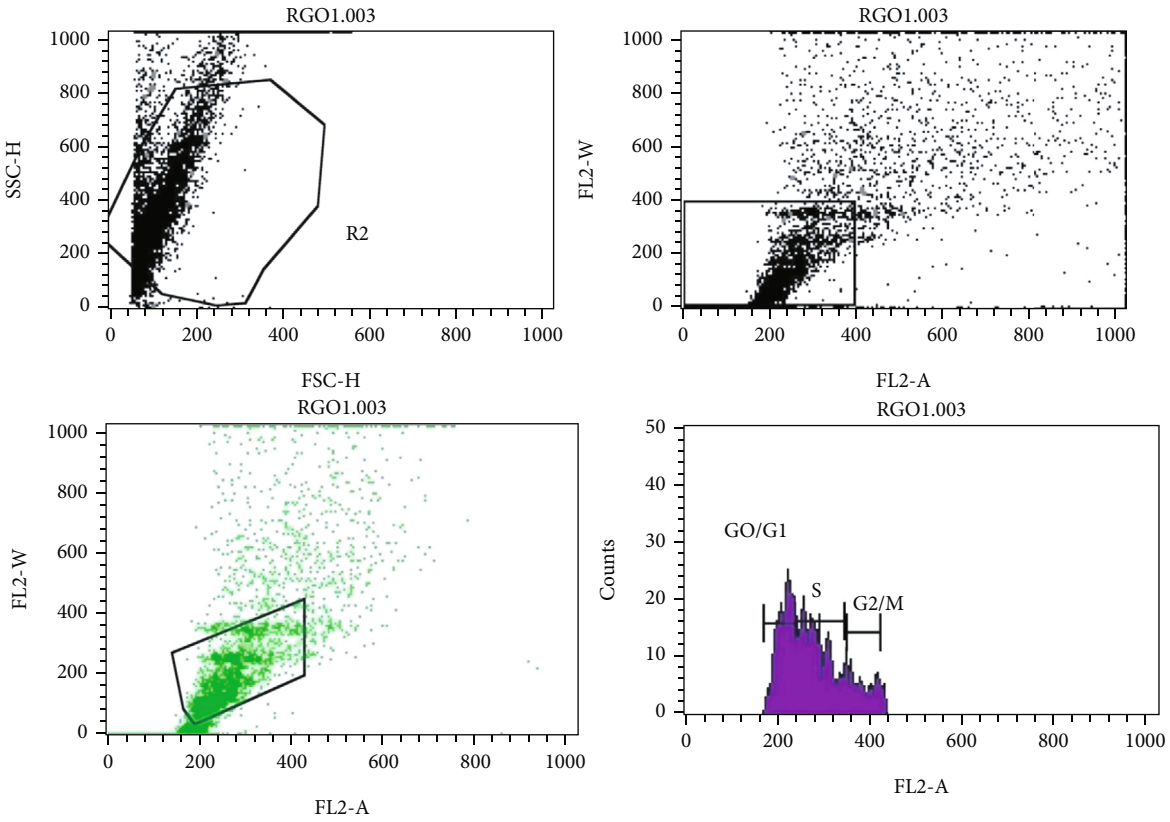

Histogram statistics

File: RGO1.003	Log data units: Linear values
Sample ID:	Patient ID:
Tube: Untitled	Panel: Untitled acquisition tube list
Acquisition date: 21-Jun-18	Gate: G1
Gated events: 1820	Total events: 10000
X Parameter: FL2-A (Linear)	

Marker	Left,	Right	Events	% Gated	% Total	Mean	Geo Mean	CV	Median	Peak Ch
All	0,	1023	1820	100.00	18.20	265.66	259.17	22.93	254.00	217
GO/G1	168,	234	697	38.30	6.97	208.72	208.17	7.23	210.00	217
S	236,	342	858	47.14	8.58	279.12	277.68	10.28	274.00	254
G2/M	347,	418	207	11.37	2.07	380.38	379.75	5.77	378.00	352

(c) T-rGO-treated cells

Figure 7: Detection of apoptosis in PC-3 human prostate cancer cells.

2.20.4. Raman Spectroscopy Analysis. Raman spectroscopy helps in determining carbon compounds' structure and nature. The G-band and D-band appearing around 1586 and1350 cm^{-1} are the most common species to distinguish between graphene derivatives. The G-band corresponds to the E_{2g} phonon of C sp^2 particles, whereas the D-band is a breathing technique of the A_{1g} symmetry k-point phonon.

As shown in Figure 4, the Raman spectrum of GO displays two main broad and low intensity bands located at 1589 cm^{-1} and 1352 cm^{-1}, corresponding to G-band and D-band, respectively. After reduction, the Raman spectrum of T-rGO displays similar G-band and D-band. It can be noticed that bands' position remains similar but there is a significant increase in the intensity, signifying an improvement of the crystallinity after the completion of reduction from GO to T-rGO. Furthermore, the $I_{D\text{-band}}/I_{G\text{-band}}$ ratios from the recorded Raman spectra are as follows: 0.96 and 1.24 for GO and T-rGO, respectively. This further confirms the completion of the reduction process of GO using thiourea induced reduction and the successful formation of T-rGO.

This relation represents a measure of structural defects. The information got from Raman spectroscopy of decreased graphene oxide accommodated a primary change because of the course of decrease; the G pinnacle and D pinnacle were both broadened and were moved to around 20 cm^{-1}, individually [68, 69].

2.20.5. TGA Analysis. Thermogravimetric analysis has been carried out under dry air to investigate the thermal

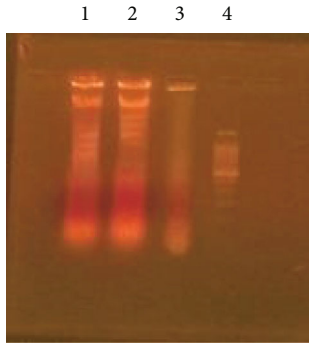

Figure 8: DNA fragmentation of PC-3 human prostate cancer cells treated with GO. T-rGO DNA was isolated from treated and untreated PC-3 cells and electrophoresis on agarose gel (lane 1, rGO; lane 2, T-rGO; lane 3, control; and lane 4, DNA marker).

characteristics of the GO nanosheets (see Figure 5). The elimination of oxygen-containing species and carbon oxidation with complete decomposition is examined as function of mass loss. For GO, the TGA curves display three distinctive stages: (I) up to 100°C with 15 wt.% corresponding to moisture content present in the samples of GO and T-rGO; (II) up to 250°C with 25 wt.% associated to the water molecules and hydroxyl group functional groups present in between the sheets of GO; and (III) above 250°C with gradual and monotonous mass reaching around 35 wt.% at 1000°C and is attributed to removal of the CO or CO_2 functional groups present at the edges of the sheets of GO.

After reduction, the TGA curve of T-rGO exhibits a different behavior, a gradual and steady mass loss reaching about 40 wt.% at 1000°C. Additionally, the TGA curves of GO and T-rGO confirm that T-rGO are more thermally stable than the GO [70].

2.21. Biological Tests

2.21.1. Induced Cytotoxicity by GO and T-rGO in PC-3 Human Prostate Cancer Cells. Figure 6 illustrates the effects of GO and T-rGO on PC-3 human prostate cancer cells viability. The WST-8 test was used to determine the vitality of PC-3 human prostate cancer cells after 24 h of exposure to various doses of GO and T-rGO.

In human prostate cancer cells, the efficacy of GO and T-rGO as potential inhibitory agents was investigated. The doses of 125 μg/mL GO and 62.5 μg/mL T-rGO caused dose-dependent reductions in cell viability corresponding to 52.80% and 50.15%, respectively. Nonetheless, T-rGO was found to be more active than GO, as shown in Tables 1 and 2. T-rGO appeared to play the role of a chemical agent in inhibiting the survival of human prostate cancer cells. Further, GO was found to be less damaging than T-rGO for a range of cancer and noncancerous cells in previous studies [71, 72]. Jaworski et al. [73] reported similar results; the viability of human glioblastoma cells was lowered by 54% at a concentration of 100 μg/mL graphene nanoplatelets.

2.21.2. Flow Cytometric Analysis of Cellular Apoptosis. The results were obtained for apoptosis detection in PC-3 human prostate cancer cells. The cell cycle analysis using flowcytometry was used to investigate the apoptotic effect of GO and T-rGO -(A Control), (B-GO treated cells) and (C-T-rGO) treated cells, which are displayed in Figure 7. The findings demonstrates that cell aptotosis was the primary source of the cell death brought on by GO and T-rGO. rGO was found to be more efficient than sample GO because to the large proportion of dead cells. PI was used to label apoptotic cells. However, staining has not been performed on normal cells using graphene [74, 75].

2.21.3. DNA Laddering. Figure 8 depicts the DNA fragmentation of PC-3 human prostate cancer cells treated with GO and T-rGO. DNA was extracted from PC-3 cells of both treated and untreated; electrophoresis was performed on an agarose gel (lane 1, T-rGO; lane 2, GO; lane 3, control; and lane 4, DNA marker).

DNA laddering was utilized to examine the DNA fragmentation caused by GO and T-rGO in human prostate cancer cells. From Figure 8, it can be observed that after 24 h of treatment, T-rGO demonstrated a greater damage to the DNA than GO, which could be associated with the presence of fewer smooth edges [76, 77].

The rapid mobility and sharp edges of graphene may explain rGO's genotoxicity. Penetration of graphene nanosheets into a cell's membrane can partially destroy the cell's membrane, resulting in cell death. The RGO protein can then interact directly with the DNA in the cell's nucleus. This is supported by experimental evidence demonstrating that the genotoxicity threshold for graphene is substantially lower than the cytotoxicity threshold, which can be explained by the direct interaction between graphene and nuclear DNA.

The difference between GO and rGO in terms of genotoxicity is that rGO may be more effective in damaging cell membranes and penetrating into cells because they are hydrophobic and have many more rough edges. They have the ability to bind directly with nuclear DNA, causing substantial genotoxicity. GO has finer edges and hydrophilic qualities, and it appears to be less powerful in terms of accessing cell compartments and reacting with DNA, resulting in the absence of genotoxic effects [77, 78].

2.21.4. Cell Morphology. Figures 9(a) and 9(b) reveal the changes of the morphology of human prostate cancer cells after 24 h of treatment with GO and T-rGO. It can be observed that the cell morphology of the control cells is unaffected. The GO-treated cells are found denser, more oval, and distended than the control cells. T-rGO-treated cells are similarly thick, oval, and gruff in appearance compared to the control cells. Following therapy with GO and T-rGO, the number of cells has been similarly reduced. The obtained results corroborate with the results in the literature. According to Yun-Jung et al. and Hinzmann et al., GO and RGO caused severe morphological alterations in human ovarian cancer cells A2780, including loss of cell shape, disruption of cell monolayers, and reduction of cell adhesion, all of which indicated reduced cell survival [79, 80].

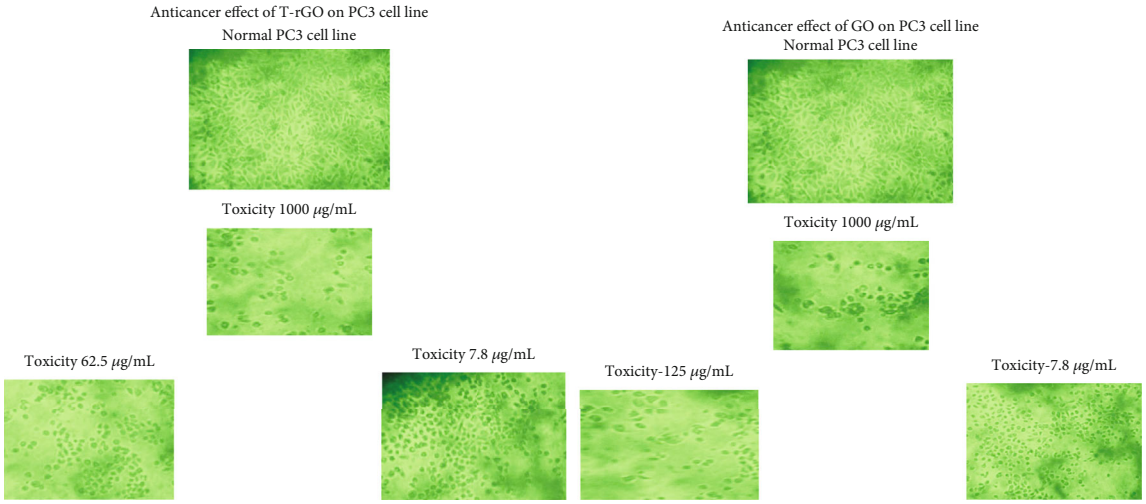

Figure 9: Morphology of PC-3 human prostate cancer cells treated with GO and reduced graphene oxide.

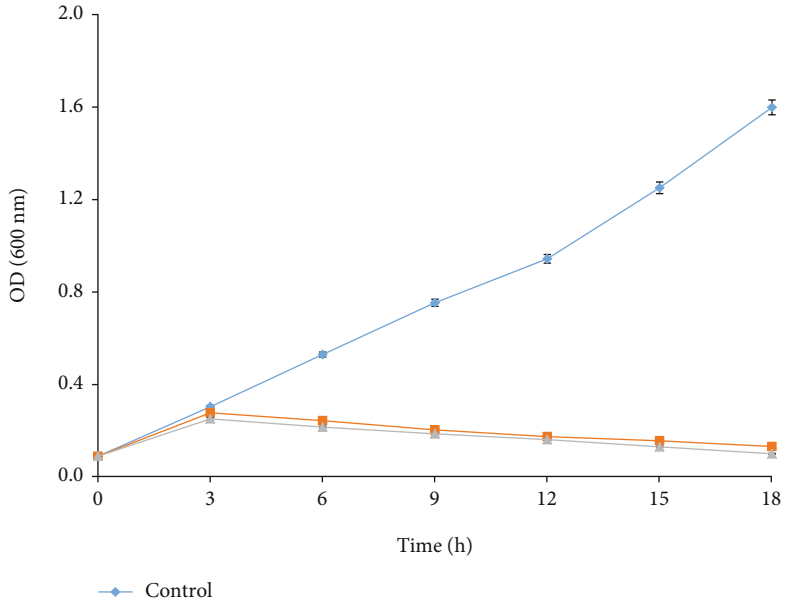

Figure 10: Effect of various graphene materials GO and T-rGO on the growth of *E. coli* mastitis bacteria.

2.21.5. Effect of GO and T-rGO on Bacterial Growth. During the first stage, the growth curve of *E. coli* mastitis bacteria in LB medium has been measured with and without GO and T-rGO (100 μg/mL) for 15 h under aerobic conditions. As a result, the exponential growth patterns of *E. coli* mastitis bacteria control strains were identical. After treatment, the cells were spun down in centrifuge, rinsed with deionized water, and assessed for culture at 600 nm. The standard deviation was represented by the error bars. Control was the isotonic saline solution without graphene-based compounds.

The effects of GO and T-rGO on *E. coli* growth are illustrated in Figure 10. It can be noted that the growth of *E. coli* was reduced after treatment with both GO and T-rGO, reaching up to 89.79% and 87.66% following 15 h treatment, respectively. The antibacterial efficacy was slightly higher for T-rGO than GO. This agrees with the literature [81, 82].

When GO was introduced to bacterial culture at 25 μg/mL, bacteria grew quicker and to a greater optical density than cultures without GO. Ruiz et al. [81] explained why bacteria grew two and three times more on filters coated with 25 and 75 μg of GO than on filters without GO. Graphene materials were found to have significant antibacterial activity by Liu et al. [82].

2.21.6. Dose-Dependent Antibacterial Efficacy of GO and T-rGO. We investigated the concentration dependence of antibacterial activity of GO and reduced graphene oxide on *Escherichia coli* mastitis bacteria in order to verify the synthesized GO and reduced graphene oxide functions. To avoid any chemical residues in LB medium, cells were cultured in LB medium, spun down, and resuspended in PBS. GO or reduced graphene oxide dispersion at various

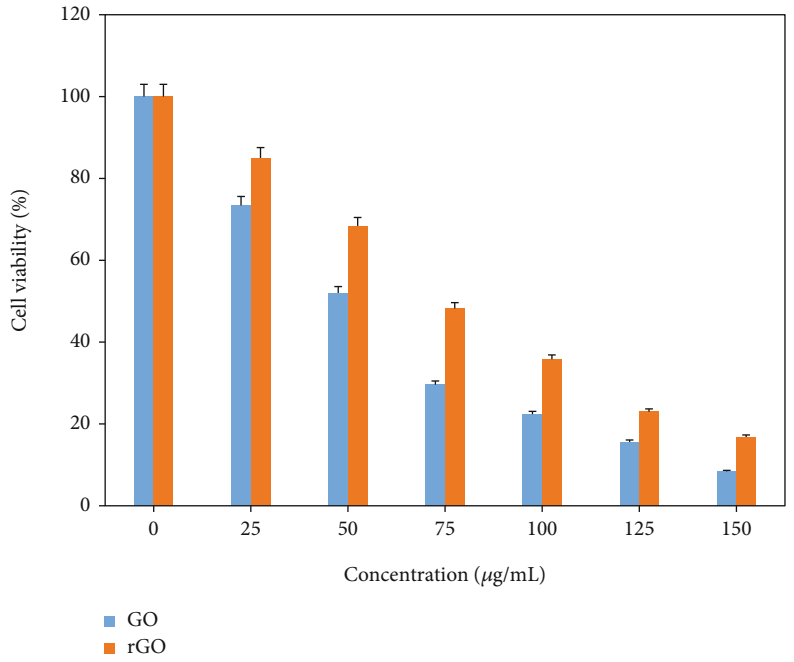

Figure 11: Effect of concentration-dependent GO and T-rGO in *E. coli* mastitis bacteria cell viability.

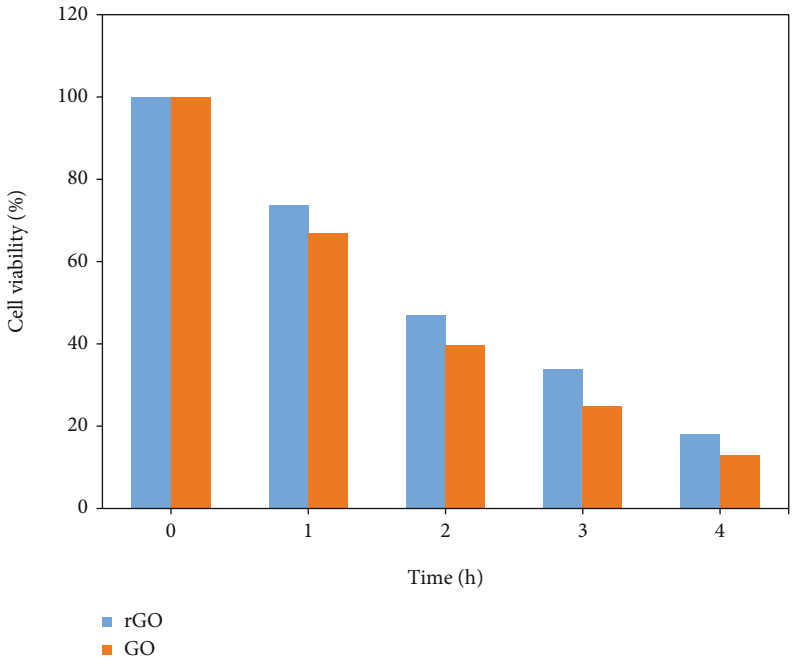

Figure 12: Cell viability in time-dependent antibacterial activities of GO and T-rGO.

concentrations (0, 25, 50, 75, 100,125,150,175, and 200 μg/mL) were used with *E. coli* mastitis bacterial cells (10^6 CFU/mL) for 2 h at 37°C with a 200 rpm shaking speed.

Figure 11 displays the dosage-based antibacterial efficacy of GO and T-rGO for *E. coli*. It can be observed that the growth of *E. coli* was reduced as the concentration of GO and T-rGO increased [83].

2.21.7. Time-Dependent Antibacterial Activity of GO and T-rGO. The antibacterial efficacy of GO and reduced graphene oxide was studied over time. With similar concentrations of cell biomass, GO and reduced graphene oxide dispersion (100 μg/mL) were cultured with *E. coli* mastitis bacteria.

At several time points such as 1, 2, 3, and 4 h, the vitality of *E. coli* mastitis bacteria was noted. After 1 h of incubation, the losses of viability of *E. coli* mastitis were 33.08% and 26.15% for GO and T-rGO, respectively. Further increase in contact time resulted in significant reduction of growth, reaching 86.92% and 81.92% for GO and T-rGO, respectively. Moreover, it was noted that the bactericidal activity

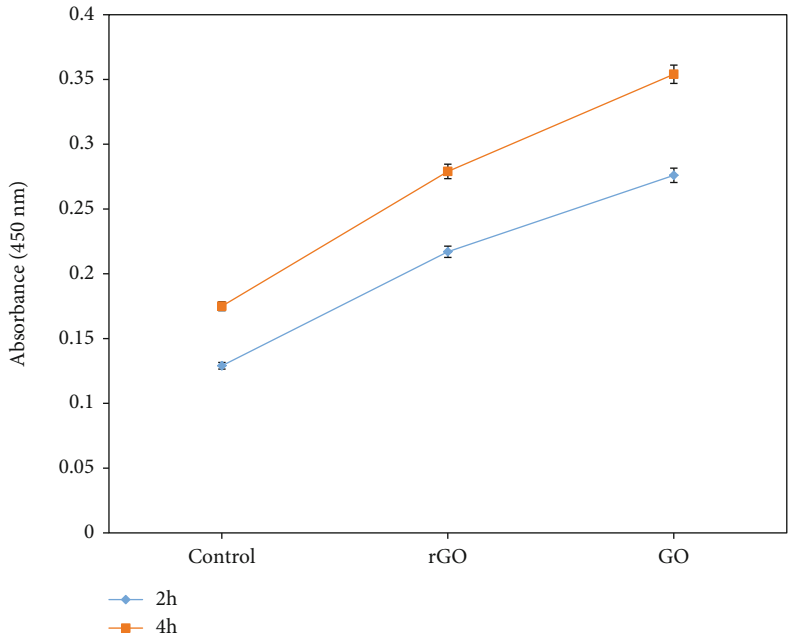

Figure 13: Production of superoxide radical anion (O2-) by GO and T-rGO dispersions.

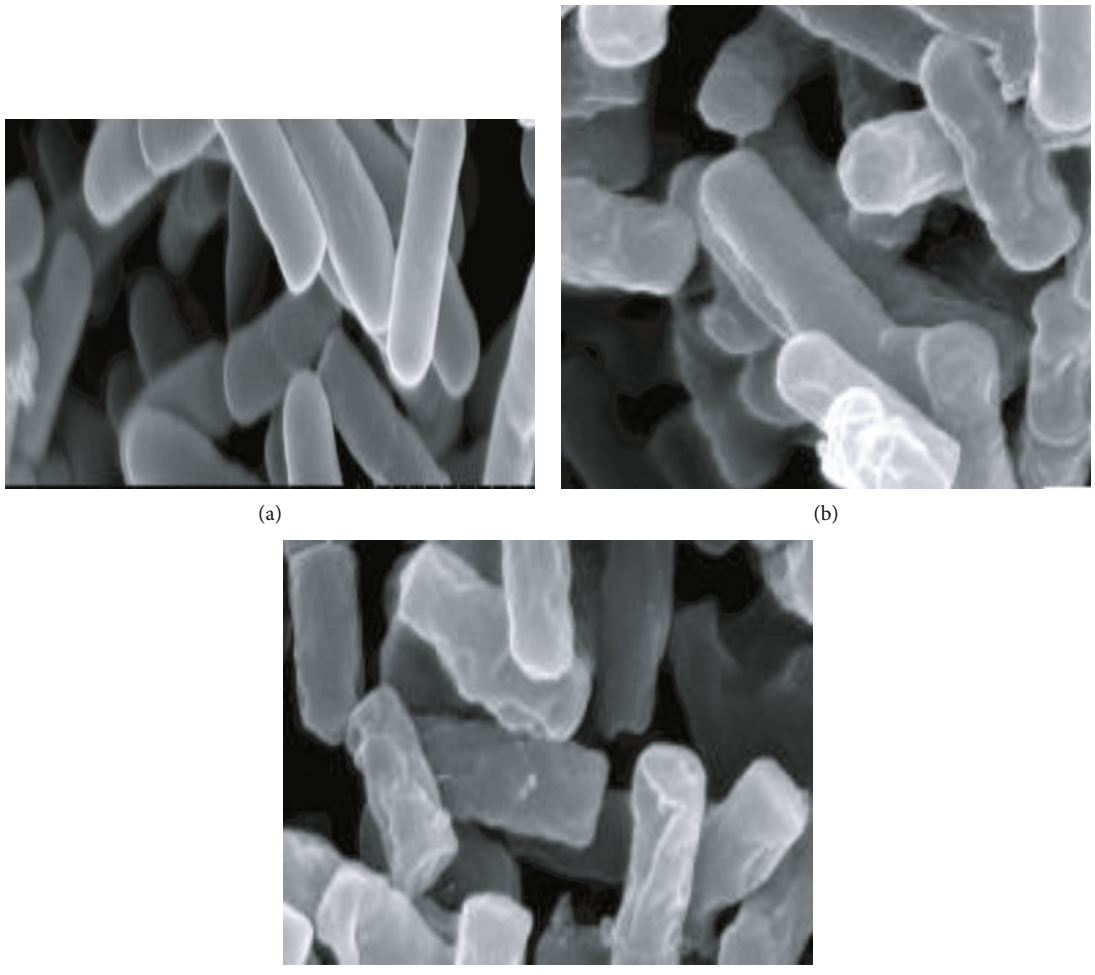

Figure 14: SEM images of Escherichia coli mastitis bacteria (a, b, c).

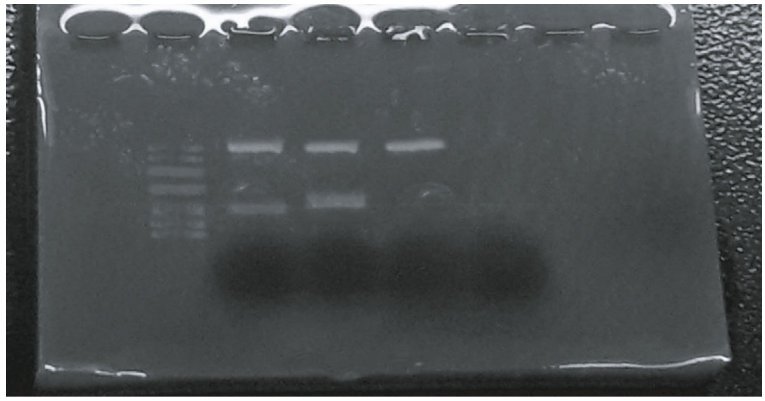

Figure 15: DNA fragmentation of *Escherichia coli* mastitis bacteria treated with GO and T-rGO.

of GO was superior to that of T-rGO. Cell death occurred in all 4 h incubation.

When comparing GO and reduced graphene oxide dispersions, we discovered that dispersions of GO had much stronger antibacterial activity than rGO dispersions at all incubation intervals evaluated. Figure 12 displays the time-dependent antibacterial activity of GO ans T-rGO cells.

2.21.8. ROS Generation. One often hypothesized toxicological mechanism of nanoparticles is the formation of reactive oxygen species (ROS). We wanted to see if graphene materials were capable of causing oxidative stress. The control cells without graphene materials had not produced any ROS.

The production of reactive oxygen species (ROS) is linked to a material's toxicity. The results are shown in Figure 13. The GO and T-rGO at 100 μg/mL increased the generation of superoxide radical anions by 2.02 and 1.6 times, respectively, after 4 h of treatment as compared to the control [77, 84, 85].

The findings suggested that the graphene nanomaterials' higher bacterial toxicity was due to more sharpening of the nanomaterials' edges, resulting in stronger contact interaction with the cell membrane and/or better charge transfer between the bacteria and the nanomaterials, resulting in more bacterial cell membrane damage.

2.21.9. Destruction of Bacterial Membranes. SEM was used to illustrate interactions between graphene-based materials and *E. coli* mastitis bacterial cells in order to determine how graphene-based materials kill bacteria. After exposure to GO or reduced graphene oxide dispersions, most *E. coli* mastitis bacterial cells flattened and lost their cellular integrity.

Nanomaterials cause membrane stress in bacterial cells, resulting in cell structure destruction; additionally, we discovered that GO dispersion produced thin layers of nanosheets, whereas reduced graphene oxide dispersion primarily contained larger aggregated particles.

E. coli mastitis bacteria mingled with GO and reduced graphene oxide in distinct ways, according to a comparison of cells interacting with GO and reduced graphene oxide.

The majority of *E. coli* mastitis bacterial cells were individually wrapped with thin layers of GO nanosheets, as seen in the figures. *E. coli* mastitis bacterial cells, on the other hand, were frequently encased in massive, reduced graphene oxide aggregates. The aggregation/dispersion of graphene-based materials might play a key role in their antibacterial properties, as evidenced by the distinct behavior of GO and reduced graphene oxide found in SEM images.

The interactions of graphene-based derivatives with *E. coli* were examined by recording SEM images before and after treatment. Figures 14(a)–14(c) depict the bacterium's interaction with the grapheme nanosheets [83].

2.21.10. DNA Laddering. To investigate whether oxidative stress could cause DNA fragmentation, which is one of the hallmarks of apoptosis and a good sign of cellular failure, DNA laddering test has been carried out.

DNA was isolated and examined from *E. coli* mastitis bacterial cells that had been treated with 100 μg/mL GO and reduced graphene oxide for 2 h.

The results demonstrated that after 2 h of treatment, neither graphene nor reduced graphene oxide-treated cells showed any significant response; nevertheless, after 6 h treatment, the cells showed a minor effect of DNA fragmentation. Surprisingly, cells exposed to GO and reduced graphene oxide for 24 h showed a significant effect of DNA fragmentation, implying that cells required a longer time exposure to GO and reduced graphene oxide to generate ROS, which led to DNA fragmentation.

Based on our findings, we infer that the antibacterial activity of GO and reduced graphene oxide was due to direct contact of *E. coli* with sharp nanosheets, resulting in the creation of reactive oxygen species (ROS) and DNA fragmentation, leading to cell death. This study revealed that GO and decreased graphene DNA breakage and cell death [86, 87].

After 2 h of treatment with 100 μg/mL of GO and T-rGO, the DNA of *E. coli* showed no changes. Mild alterations were observed after 6 h of treatment. Surprisingly, DNA fragmentation occurred only after 24 h. This was demonstrated through DNA laddering, as reported in the literature [86–88]. Figure 15 displays the DNA fragmentation of E. Coli mastitis bacteria treated with GO and T-rGO.

3. Conclusion

In a variety of biological applications, such as cancer treatment, bacterial control, viral inactivation, and drug administration, graphene and materials linked to it are frequently used. The present study shows a straightforward method for producing GO and rGO from graphene by employing thiourea. The physiochemical characteristics of GO and T-rGO were investigated using XRD, SEM, FTIR, Raman spectroscopy, and TGA.

According to the results, GO and T-rGO nanosheets showed cytotoxicity and caused cell death in human prostate cancer cells. The obtained results showed that rGO was cytotoxic at concentrations as low as 62.5 μg/mL. Furthermore, these results are better than that reported by Kretowski et al., where the cytotoxicity was found to occur at a minimum concentration of 100 μg/mL [89].

Additionally, reactive oxygen species were produced, and DNA fragmentation was brought on by the interaction of GO and T-rGO nanosheets with E. coli. Additionally, it was discovered that GO and T-rGO damage bacterial cells. These findings imply that GO and T-rGO could both be utilized as pharmacological agents in therapeutic procedures.

Additionally, functionalized nanoparticle composites and drug/siRNA-mediated combination therapy may defeat induced mutagenesis and frequently recurrent cancers brought on by chemotherapeutic agents, indicating that the functionalized nanoparticle composites may be used as adjuvant agents to enhance the therapeutic effect thus treat cancer and bacterial cells. Clinically, the elimination of all cancer and bacterial cells may be facilitated by a novel therapy that combines nanoparticles with a medication or siRNA that targets cancer-initiating cells. Additionally, this graphene-based compound (a medicine with nanoparticles enclosed) has great benefits as a powerful antibacterial and anticancer agent. However, more research is necessary to shed light at the molecular level to examine in more detail the actions of drug/siRNA-mediated combination therapy, functionalized nanoparticle composites, cancer, and bacterial cells.

Additionally, nanoparticle-mediated therapy can treat cancers that have repeatedly relapsed due to induced cell death, mutation, and chemotherapeutic agent-caused mutagenesis. In the clinical setting, a combination therapy using nanoparticles and a medication that specifically targets tumor-initiating cells will probably make it easier to eradicate dead cancer cells.

This study offers potential redox biological mechanisms, gene modulations involved in cell death, and significant signalling pathways like cell survival and cell death. However, more research is necessary to better elucidate at the chemical and biological levels for graphene's diverse effects on tumor cells.

Because of their exceptional characteristics, including large specific surface area and outstanding physicochemical properties, graphene and its derivatives are gaining more and more interest for their potential use in bone tissue engineering. Nonetheless, further research is necessary to be carried out on graphene nanocomposites and related molecular biology mechanisms.

Data Availability

Data is available in this manuscript

Conflicts of Interest

Data available in the manuscrpt is not applicable.

Acknowledgments

The authors are grateful to Anna University and Loyola College for the infrastructural facilities and support offered in completing the present work.

References

[1] K. N. Thakkar, S. S. Mhatre, and R. Y. Parikh, "Biological synthesis of metallic nanoparticles," *Nanomedicine*, vol. 6, no. 2, pp. 257–262, 2010.

[2] A. K. Geim and K. S. Novoselov, "The rise of graphene," *Natural Materials*, vol. 6, no. 3, pp. 183–191, 2007.

[3] H. P. Boehm, A. Clauss, V. Hofmann, and G. O. Fischer, "Dunnstehohlenstoff-Folien Zeitschrift Fur Naturforschung part B," *Chemie Biochemie Biophysik Biologie und verwandten Gebiete*, vol. 17, no. 3, pp. 150–153, 1962.

[4] P. R. Wallace, "The band theory of graphite," *PhysicsReview*, vol. 71, no. 9, pp. 622–634, 1947.

[5] J. W. McCure, "Diamagnetism of graphite," *Physics Review*, vol. 104, no. 3, pp. 666–671, 1956.

[6] G. W. Semenoff, "Condensed-matter simulation of a three-dimensional anomaly," *Physics Review Letters*, vol. 53, no. 26, pp. 2449–2452, 1984.

[7] K. S. Novoselov, A. K. Geim, S. V. Morozov et al., "Electric field effect in atomically thin carbon films," *Science*, vol. 306, no. 5696, pp. 666–669, 2004.

[8] K. S. Novoselov, D. Jiang, F. Schedin et al., "Two-dimensional atomic crystals," *Proceedings of the National Academy of Sciences of the United States of America*, vol. 102, no. 30, pp. 10451–10453, 2005.

[9] C. Lee, X. Wei, J. W. Kysar, and J. Hone, "Measurement of the elastic properties and intrinsic strength of monolayer graphene," *Science*, vol. 321, no. 5887, pp. 385–388, 2008.

[10] D. Li, M. B. Mulller, S. Gulje, R. B. Kaner, and G. G. Wallace, "Processable aqueous dispersions of graphene nanosheets," *Nature Nanotechnology*, vol. 3, no. 2, pp. 101–105, 2008.

[11] Y. Zhu, S. Murali, W. Cai, and S. Rodeny Ruoff, "Graphene and graphene oxide: synthesis, properties, and applications," *Advanced Materials*, vol. 22, no. 35, pp. 3906–3924, 2010.

[12] K. I. Bolotin, K. J. Sikes, Z. Jiang et al., "Ultrahigh electron mobility in suspended graphene," *Solid State Communication*, vol. 146, no. 9-10, pp. 351–355, 2008.

[13] N. O. Weiss, H. Zhou, L. Liao et al., "Graphene: an emerging electronic material," *Advanced Materials*, vol. 24, no. 43, pp. 5782–5825, 2012.

[14] X. An, W. Thomas Butler, M. Washinton, and S. Kar, "Optical and sensing properties of 1-pyrenecarboxylic acid-functionalized graphene films laminated on polydimethylsiloxane membranes," *ACS Nano*, vol. 5, no. 2, pp. 1003–1011, 2011.

[15] A. A. Balandin, S. Ghosh, W. Bao, I. Calizo, and F. Miao, "Superior thermal conductivity of single-layer graphene," *Nano Letters*, vol. 8, no. 3, pp. 902–907, 2008.

[16] V. Geogakilas, M. Otyepka, B. A. Bourlinos, and K. Christian Kemp, "Functionalization of graphene: covalent and non-covalent approaches, derivatives and applications," *Chemical Reviews*, vol. 112, no. 11, pp. 6156–6214, 2012.

[17] X. Hunag, F. Boey, and H. Zhang, "Graphene-based composites," *Chemical Society Reviews*, vol. 41, no. 2, 2012.

[18] M. D. Stoller, S. Park, Y. Zhu, J. An, and R. S. Ruoff, "Graphene-based ultracapacitors," *Nano Letters*, vol. 8, no. 10, pp. 3498–3502, 2008.

[19] Z. Chen, W. Ren, L. Gao, B. Liu, S. Pei, and H. Cheng, "Three-dimensional flexible and conductive interconnected graphene networks grown by chemical vapour deposition," *Nature Materials*, vol. 10, no. 6, pp. 424–428, 2011.

[20] D. A. Dikin, S. Stankovich, E. J. Zimney et al., "Preparation and characterization of graphene oxide paper," *Nature*, vol. 448, no. 7152, pp. 457–460, 2007.

[21] S. Park, K. S. Lee, G. Bozoklu, W. Cai, S. B. T. Nguyen, and R. S. Ruoff, "Graphene oxide papers modified by divalent ions-enhancing mechanical properties via chemical cross-linking," *ACS Nano*, vol. 2, no. 3, pp. 572–578, 2008.

[22] S. Stankovich, H. B. Dikin Geoffrey, T. Nguyen, S. Rodney Ruoff, and A. Eric, "Graphene-based composite materials," *Nature*, vol. 442, no. 7100, pp. 282–286, 2006.

[23] T. Ramanathan, A. A. Abdala, S. Stankovich et al., "Functionalized graphene sheets for polymer nanocomposites," *Nature Nanotechnology*, vol. 3, no. 6, pp. 327–331, 2008.

[24] P. Blake, P. D. Brimicombe, R. R. Nair et al., "Graphene-based liquid crystal device," *Nano Letters*, vol. 8, no. 6, pp. 1704–1708, 2008.

[25] J. S. Bunch, M. Arend van der Zande, S. Scott Verbridge, and W. Ian Frank, "Electromechanical resonators from graphene sheets," *Science*, vol. 315, no. 5811, pp. 490–493, 2007.

[26] B.-Y. Lu, G.-Y. Zhu, C. H. Yu et al., "Functionalized graphene oxide nanosheets with unique three-in-one properties for efficient and tunable antibacterial applications," *Nano Research*, vol. 14, no. 1, pp. 185–190, 2021.

[27] C.-H. Yu, G.-Y. Chen, M.-Y. Xia et al., "Understanding the sheet size-antibacterial activity relationship of graphene oxide and the nano-bio interaction-based physical mechanisms," *Colloids and Surfaces. B, Biointerfaces*, vol. 191, article 111009, 2020.

[28] H. Shen, L. Zhang, M. Liu, and Z. Zhang, "Biomedical applications of graphene," *Theranostics*, vol. 2, no. 3, pp. 283–294, 2012.

[29] A. Omid and E. Ghaderi Shahavar, "Graphene nanogrids for selective and fast osteogenic differentiation of human mesenchymal stem cells," *Carbon*, vol. 59, pp. 200–211, 2013.

[30] S. Matis, I. Kalt, A. Gedanken, and R. Sarid, "Herpes simplex virus type-1 attachment inhibition by functionalized graphene oxide," *ACS applied materials & interfaces*, vol. 6, pp. 1228–1235, 2014.

[31] S. Agarwal, X. Zhou, F. Ye et al., "Interfacing live cells with nanocarbon substrates," *Langmuir*, vol. 26, no. 4, pp. 2244–2247, 2010.

[32] N. Li, X. Zhang, Q. Song et al., "The promotion of neurite sprouting and outgrowth of mouse hippocampal cells in culture by graphene substrates," *Biomaterials*, vol. 32, no. 35, pp. 9374–9382, 2011.

[33] C. Heo, J. Yoo, S. Lee et al., "The control of neural cell-to-cell interactions through non-contact electrical field stimulation using graphene electrodes," *Biomaterials*, vol. 32, no. 1, pp. 19–27, 2011.

[34] X. Sun, Z. Liu, K. Welsher, J. Robinson, A. Goodwin, and H. Dai, "Nano-graphene oxide for cellular imaging and drug delivery," *Nano Research*, vol. 1, no. 3, pp. 203–212, 2008.

[35] J. Liu, J. Dong, T. Zhang, and Q. Peng, "Graphene-based nanomaterials and their potentials in advanced drug delivery and cancer therapy," *Journal of Controlled Release*, vol. 286, pp. 64–73, 2018.

[36] K. Ostrikov, E. C. Neyts, and M. Meyyappan, "Plasma nanoscience: from nano-solids in plasmas to nano-plasmas in solids," *Advanced Physics*, vol. 62, no. 2, pp. 113–224, 2013.

[37] R. Lulu, Y. Zhang, C. Cui, Y. Bi, and X. Ge, "Functionalized graphene oxide for anti-VEGF siRNA delivery: preparation, characterization and evaluation in vitro and in vivo," *RSC Advances*, vol. 7, pp. 20553–20566, 2017.

[38] Y. Ting, H. Zhang, D. Huang, S. Feng, M. Fujita, and X.-D. Gao, "Chitosan-Functionalized graphene oxide as a potential Immunoadjuvant," *Immunoadjuvant Nanomaterials*, vol. 7, no. 3, p. 59, 2017.

[39] C. Huo, Y. H. Kao, and C. P. Chu, "Androgen receptor inhibits epithelial-mesenchymal transition, migration, and invasion of PC-3 prostate cancer cells," *Cancer Letters*, vol. 369, no. 1, pp. 103–111, 2015.

[40] S. M. Kim, E. Y. Oh, J. H. Lee et al., "Brassinin combined with capsaicin enhances apoptotic and anti-metastatic effects in PC-3 human prostate cancer cells," *Phytotherapy Research*, vol. 29, no. 11, pp. 1828–1836, 2015.

[41] F. Z. Shahneh, B. Baradaran, J. Majidi, and Z. Babaloo, "Echinophora platyloba DC (Apiaceae) crude extract induces apoptosis in human prostate adenocarcinoma cells (PC-3)," *Biomedical Journal*, vol. 37, no. 5, pp. 298–304, 2014.

[42] O. M. Radostitis, C. C. Gay, D. Blood, and K. W. Hinchkliff, *VeterinaryMedicine*, ELBS and Baillier Tindall, 9th edition, 2000.

[43] N. Sharma, G. J. Rho, Y. H. Hong et al., "Bovine mastitis: an Asian perspective," *Asian Journal of Animal and Veterinary Advances*, vol. 7, no. 6, pp. 454–476, 2012.

[44] S. J. LeBlanc, K. D. Lissemore, D. F. Kelton, T. F. Duffield, and K. E. Leslie, "Major advances in disease prevention in dairy cattle," *Journal of Dairy Science*, vol. 89, no. 4, pp. 1267–1279, 2006.

[45] G. Y. Miller, P. C. Barlet, S. E. Lance, J. Anderson, and L. E. Heider, "Costs of clinical mastitis and mastitis prevention in dairy herds," *Journal of the American Veterinary Medical Association*, vol. 202, no. 8, pp. 1230–1236, 1993.

[46] W. S. Hummers and R. E. Offeman, "Preparation of graphitic oxide," *Journal of the American Chemical Society*, vol. 80, no. 6, pp. 1339–1339, 1958.

[47] S. Gurunathan, J. W. Han, V. Eppakayala, and J. H. Kim, "Microbial reduction of graphene oxide by Escherichia coli: a green chemistry approach," *Colloids Surface B Biointerfaces*, vol. 102, no. 1, pp. 772–777, 2013.

[48] S. Gurunathan, J. Han, and J. H. Kim, "Humanin: a novel functional molecule for the green synthesis of graphene," *Colloids Surface B Biointerfaces*, vol. 111, pp. 376–383, 2013.

[49] S. Gurunathan, J. Han, J. H. Park, and J. H. Kim, "An in vitro evaluation of graphene oxide reduced by Ganoderma spp. in

human breast cancer cells (MDA-MB-231)," *International Journal of Nanomedicine*, vol. 9, pp. 1783–1797, 2014.

[50] G. Prasannaraj, S. V. Sahi, S. Ravikumar, and P. Venkatachalam, "Enhanced cytotoxicity of biomolecules loaded metallic silver nanoparticles against human liver (HepG2) and prostate (PC3) cancer cell lines," *Journal of Nanoscience and Nanotechnology*, vol. 16, no. 5, pp. 4948–4959, 2016.

[51] H. Tom, L. Baruch, and M. Machluf, "Ultrsound-mediated mesenchymal stem cells transfection as a targeted cancer therapy platform," *Scientific Reports*, vol. 7, p. 42046, 2017.

[52] S. Gurunathan, J. W. Han, V. Eppakayala, and J. H. Kim, "Green synthesis of graphene and its cytotoxic effects in human breast cancer cells," *International Journal of Nanomedicine*, vol. 8, no. 1, pp. 1015–1027, 2013.

[53] K. H. Liao, Y. S. Lin, C. W. Macosko, and C. L. Haynes, "Cytotoxicity of graphene oxide and graphene in human erythrocytes and skin fibroblasts," *ACS Applied Materials & Interfaces*, vol. 3, no. 7, pp. 2607–2615, 2011.

[54] K. Yiyuan, J. Liu, J. Wu et al., "Graphene oxide and reduced graphene oxide induced neuropheochromocytoma-derived PC12 cell lines apoptosis and cell cycle alterations via the ERK signaling pathways," *International Journal of Nanomedicine*, vol. 12, pp. 5501–5510, 2017.

[55] A. H. Wyllie, "Glucocorticoid-induced thymocyte apoptosis is associated with endogenous endonuclease activation," *Nature*, vol. 284, no. 5756, pp. 555-556, 1980.

[56] A. H. Wyllie, J. F. R. Kerr, and A. R. Currie, "Cell death: the significance of apoptosis," *International Review of Cytology*, vol. 68, pp. 251–306, 1980.

[57] W. Hao, W. Gu, N. Xiao, L. Ye, and Q. Xu, "Chlorotoxin-conjugated graphene oxide for targeted delivery of an anticancer drug," *International Journal of Nanomedicine*, vol. 9, pp. 1433–1442, 2014.

[58] O. Klastrup, "Scandinavian recommendations on examination of quarter milk samples," *Proc. IDF Seminar on mastitis Control. Int. Dairy Fed*, F. H. Dodd, Ed., vol. 85, pp. 49–52, 1975.

[59] S. Gurunathan, K. Kaliswaralal, R. Vaidyanathan, D. Venkataraman, S. R. Pandian, and J. Muniyandi, "Biosynthesis, purification and characterization of silver nanoparticles using Escherichia coli," *Colloids and Surface*, vol. 74, no. 1, pp. 328–335, 2009.

[60] N. Gurbani, C. P. Han, K. Marumoto, R. S. Liu, R. J. Choudhary, and N. Chouhan, "Biogenic reduction of graphene oxide: an efficient superparamagnetic material for photocatalytic hydrogen production," *ACS Appl. Energy Mater.*, vol. 1, no. 11, pp. 5907–5918, 2018.

[61] H. Kumar, P. N. Tengli, V. K. Mishra, P. Tripathi, A. Bhushan, and P. K. Mishra, "The effect of reduced graphene oxide on the catalytic activity of Cu–Cr–O–TiO2to enhance the thermal decomposition rate of ammonium perchlorate: an efficient fuel oxidizer for solid rocket motors and missiles," *RSC Advances*, vol. 7, no. 58, pp. 36594–36604, 2017.

[62] F. T. Thema, M. J. Moloto, E. D. Dikio, N. N. Nyangiuwe, L. Kotsedi, and M. K. Maaza, "Synthesis and characterization of graphene thin films by chemical reduction of exfoliated and intercalated graphite oxide," *Journal of Chemistry*, vol. 2013, Article ID 150536, 6 pages, 2013.

[63] Y. Wang, P. Zhang, C. F. Liu, L. Zhan, Y. F. Li, and C. Z. Hunag, "Green and easy synthesis of biocompatible graphene for use as an anticoagulant," *RSC Advances*, vol. 2, no. 6, pp. 2322–2328, 2012.

[64] H. K. Jeong, Y. P. Lee, R. J. Lahaye et al., "Evidence of graphitic AB stacking order of graphite oxides," *Journal of the American Chemical Society*, vol. 130, no. 4, pp. 1362–1366, 2008.

[65] P. Lian, X. Zhu, S. Liang, Z. Li, W. Yang, and H. Wang, "Large reversible capacity of high quality graphene sheets as an anode material for lithium-ion batteries," *ElectrochimicaActa*, vol. 55, no. 12, pp. 3909–3914, 2010.

[66] R. S. Dey, S. Hajra, R. K. Sahu, C. R. Raj, and M. K. Panigrahi, "A rapid room temperature chemical route for the synthesis of graphene: metal-mediated reduction of graphene oxide," *Chemical Communication*, vol. 48, no. 12, pp. 1787–1789, 2012.

[67] M. Wojtoniszak, X. Chen, R. J. Kalenczuk et al., "Synthesis, dispersion, and cytocompatibility of graphene oxide and reduced graphene oxide," *Colloids Surface B Biointerfaces*, vol. 89, pp. 79–85, 2012.

[68] O. Akhavan and E. Ghader, "Photocatalytic reduction of graphene oxide nanosheets on TiO_2 thin film for photoinactivation of bacteria in solar light irradiation," *Journal of Physical Chemistry A*, vol. 113, no. 47, pp. 20214–20220, 2013.

[69] P. Wang, Z. G. Liu, X. Chen, F. L. Meng, J. H. Liu, and X. J. Huang, "UV irradiation synthesis of an AU-graphene nanocomposite with enhanced electrochemical sensing properties," *Journal of Materials Chemistry A*, vol. 1, no. 32, pp. 9189–9195, 2013.

[70] H. Hu, X. Wang, F. Liu, J. Wang, and C. Xu, "Rapid microwave-assisted synthesis of graphene nanosheets–zinc sulfide nanocomposites: optical and photocatalytic properties," *Synthetic Metals*, vol. 161, no. 5-6, pp. 404–410, 2011.

[71] N. R. Wilson, P. A. Pandey, R. Beanland et al., "Graphene oxide: structural analysis and application as a highly transparent support for electron microscopy," *ACS Nano*, vol. 3, no. 9, pp. 2547–2556, 2009.

[72] S. Gurunathan, J. W. Han, V. Eappakayala, and J. H. Kim, "Biocompatibility of microbially reduced graphene oxide in primary mouse embryonic fibroblast cells," *Colloids Surface B Biointerfaces*, vol. 105, pp. 58–66, 2013.

[73] Y. Zhang, S. F. Ali, E. Dervishi et al., "Cytotoxicity effects of graphene and single-wall carbon nanotubes in neural phaeochromocytoma-derived PC12 cells," *ACS Nano*, vol. 4, no. 6, pp. 3181–3186, 2010.

[74] S. Jaworski, E. Sawosz, M. Grodzik et al., "In vitro evaluation of the effects of graphene platelets on glioblastoma multiforme cells," *International Journal of Nanomedicine*, vol. 8, pp. 413–420, 2013.

[75] K. Ishikawa, H. Ishii, and T. Saito, "DNA damage-dependent cell cycle checkpoints and genomic stability," *DNA Cell Biology*, vol. 25, no. 7, pp. 406–411, 2006.

[76] M. Kucki, L. Diener, N. Bohmer et al., "Uptake of label-free graphene oxide by Caco-2 cells is dependent on the cell differentiation status," *Journal of Nanobiotechnology*, vol. 15, no. 1, p. 46, 2017.

[77] O. Akhavan, E. Ghaderi, and A. Akhavan, "Size-dependent genotoxicity of graphene nanoplatelets in human stem cells," *Biomaterials*, vol. 33, no. 32, pp. 8017–8025, 2012.

[78] O. Akhavan, E. Ghaderi, H. Emamy, and F. Akahavan, "Genotoxicity of graphene nanoribbons in human mesenchymal stem cells," *Carbon*, vol. 54, pp. 419–431, 2013.

[79] Y. J. Choi, E. Kim, J. W. Han, J. H. Kim, and S. Gurunathan, "A novel biomolecule-mediated reduction of graphene oxide: a multifunctional anti-cancer agent," *Molecules*, vol. 21, no. 3, p. 375, 2016.

[80] M. Hinzmann, S. Jaworski, M. Kutwin, and G. Sawosz, "Nanoparticles containing allotropes of carbon have genotoxic effects on glioblastoma multiforme cells," *International Journal of Nanomedicine*, vol. 9, pp. 2409–2417, 2014.

[81] O. N. Ruiz, K. A. Fernando, B. Wang et al., "Graphene oxide: a nonspecific enhancer of cellular growth," *ACS Nano*, vol. 5, no. 10, pp. 8100–8107, 2011.

[82] G. Yujie, D. Yuanhao, C. Yubin et al., "Graphene oxide nanosheets with efficient antibacterial activity against methicillin-resistant Staphylococcus aureus (MRSA)," *Journal of Biomedical Nanotechnology*, vol. 17, pp. 1627–1634, 2021.

[83] W. Hu, C. Peng, W. Luo et al., "Graphene-based antibacterial paper," *ACS Nano*, vol. 4, no. 7, pp. 4317–4323, 2010.

[84] O. Akhavan, E. Ghaderi, and K. Rahimi, "Adverse effects of graphene incorporated in TiO_2 photocatalyst on minuscule animals under solar light irradiation," *Journal of Materials Chemistry*, vol. 22, no. 43, p. 23260, 2012.

[85] A. C. Ferrari, J. C. Meyer, V. Scardaci et al., "Raman spectrum of graphene and graphene layers," *Physical Review Letters*, vol. 97, no. 18, article 187401, 2006.

[86] M. Valko, C. J. Rhodes, J. Monocol, and M. Mazur, "Free radicals, metals and antioxidants in oxidative stress-induced cancer," *Cancer Chemistry and Biological Interactions*, vol. 160, no. 1, pp. 1–40, 2006.

[87] M. Otto, V. Gogvadez, S. Orrenius, and B. Zhivotovsky, "Mitochondria, oxidative stress and cell death," *Apoptosis*, vol. 12, no. 5, pp. 913–922, 2007.

[88] M. Yengxia, Y. Xie, C.-H. Yu et al., "Graphene-based nanomaterials: the promising active agents for antibiotics- independent antibacterial applications," *Journal of Controlled Release*, vol. 307, pp. 16–31, 2019.

[89] R. Kretowski, A. Jablonska-Tyrypuc, and M. Cechowska-Pasko, "The preliminary study on the proapoptotic effect of reduced graphene oxide in breast cancer cell lines," *International Journal of Molecular Sciences*, vol. 22, no. 22, p. 12593, 2021.